Active flow control with unsteady Coanda actuation on a high-lift configuration

Y. El Sayed M.[1], N. C. Gomes de Paula[2], B. Genest[3], R. Semaan[4] and R. Radespiel[5]
Technische Universität Braunschweig, Institute of Fluid mechanics, Hermann-Blenk-Str. 37 38108 Braunschweig, Germany

J. Petersen[6], C. Behr[7] and P. Wierach[8]
German Aerospace Center (DLR), Lilienthalplatz 7, Braunschweig, 38108.

B. Noack[9]
Laboratoire d'Informatique pour la Mécanique et les Sciences de l'Ingénieur, LIMSI-CNRS, Rue John von Neumann,Campus Universitaire d'Orsay, Bât 508, F-91403 Orsay, France

I. Introduction

Active flow control (AFC) with two-dimensional (e.g. Greenblatt & Wygnanski [1], Barros et al. [2] , and Chabert et al.[3]) and three-dimensional (segmented) [7–9] periodic forcing has been proven to bring aerodynamic benefits. These benefits stem from the actuation power reductions obtained compared to steady actuation. The success of periodic actuation is rooted in its exploitation of the flow instabilities, contrary to steady actuation which attempts to alter the flow topology by momentum injection. Despite its proven benefits, simple (ON/OFF) switching periodic actuation often does not deliver large enough aerodynamic gains. This paper experimentally investigates the possible combined benefits that a superimposed steady, unsteady, and spanwise-varied Coanda actuation has on a high-lift configuration. Machine learning control is also investigated as a possible approach to further increase lift gains.

For aircraft, circulation control in combination with high-lift devices offers several advantages over traditional high-lift configurations. The basic concept of circulation control involves the Coanda principle, where energy is introduced into the flow by means of a thin jet ejected tangentially from a slot near the trailing edge. The main advantage of circulation control is an increased lift output, which makes shorter take-offs and landings possible. This technology was first patented by Davidson [10] in 1960 and has since been repeatedly investigated (Lachmann [12], Wood & Nielson [13], Nielson & Biggers [15], and Englar [16]). A circulation control wing (CCW) with steady jets, even at very small mass flow rates, has been shown to yield lift coefficients that are comparable or superior to conventional high-lift systems (Sexstone et al. [21], Smith [22]). A particular variation of circulation control is the Coanda flap, where the objective is to keep the flow attached over a highly deflected flap by blowing a jet tangentially over its specially designed upper surface. This concept has been previously investigated and geometrically optimized in several previous studies [23, 24].

Efficiency requirements demand that the lift gained through the use of circulation control be as large as possible in comparison to the momentum coefficient of the blown jet, which is usually acquired by engine bleed. This ratio is referred to as the lift gain factor. An increase in the lift gain factor can be achieved through periodic blowing. Two studies during the mid-1970's investigated pulsed blowing associated with circulation control (Oyler & Palmer [25], Walters et al. [26]). Results from these experiments indicated that pulsed blowing reduced the mass requirements for CCW. Periodic blowing on a circulation control wing with circular trailing edge has also been examined (e.g. Jones et al. [27]). A 50% reduction in the required mass flow for a required lift coefficient was achieved. Recently, Semaan

[1] Research Assistant, Institute of Fluid Mechanics, TU Braunschweig.
[2] Research Assistant, Institute of Fluid Mechanics, TU Braunschweig.
[3] Assisting Student, Institute of Fluid Mechanics, TU Braunschweig.
[4] Head of Workgroup Flow Modelling and Control, Institute of Fluid Mechanics, TU Braunschweig.
[5] Head of Institute, Institute of Fluid mechanics, Institute of Fluid Mechanics, TU Braunschweig.
[6] Research Assistant, Institute of Composite Structures and Adaptive Systems.
[7] Research Assistant, Institute of Composite Structures and Adaptive Systems.
[8] Vice director of the Institute of Composite Structures and Adaptive Systems.
[9] Research Director CNRS.

et al.[17] have experimentally demonstrated the benefits of superimposing a spanwise synchronous forcing component onto the steady one for the same high-lift configuration as the current study.

Another possible increase in the lift gain factor can be achieved by adding spanwise variation to the actuation (e.g. standing or travelling wave). In this study, the spanwise variation is achieved by phase-shifting the periodic oscillation of adjacent lip segments (details in section II C), which are installed over the Coanda blowing slit. The motivation behind this new actuation concept is driven by previous successes of other comparable actuation methods, such as sweeping jets [28], vortex generators jets [30–32], and segmented pulsed blowing [7–9], where longitudinal vortices were reported to increase mixing and lift. We hypothesize that the the phase-shift at the exit slit produces a differential velocity gradient that forces the generation of streamwise vortices and thereby increases mixing and lift.

As previously mentioned, pulsed (ON/OFF) actuation (e.g. with zero net mass flux actuators, or solenoid switching valves) does not always yield the desired authority or lift gain (e.g. Chabert et al. [3], Hsiao et al. [33]). In this study, we experimentally investigate the possible lift gains from superimposed steady, unsteady, and spanwise-varied Coanda actuation. Due to the high actuation parameter space, the parametric study investigating the best actuation settings is conducted using latin hypercube sampling. These initial results show lift gains from superimposing a spanwise-synchronous (two-dimensional) periodic component onto the steady blowing component. Even higher lift gains are achieved with spanwise-varied (three-dimensional) traveling wave actuation. On the other hand, initial tests with machine-learning control showed no clear benefits over the best open-loop control results. This can be attributed to both hardware (actuators shifting) as well as software (settings) failings. Further improvements on the experimental model and on the algorithm are expected to improve the closed-loop control results during the next measurement campaign.

II. Experimental Setup

A. Experimental Model

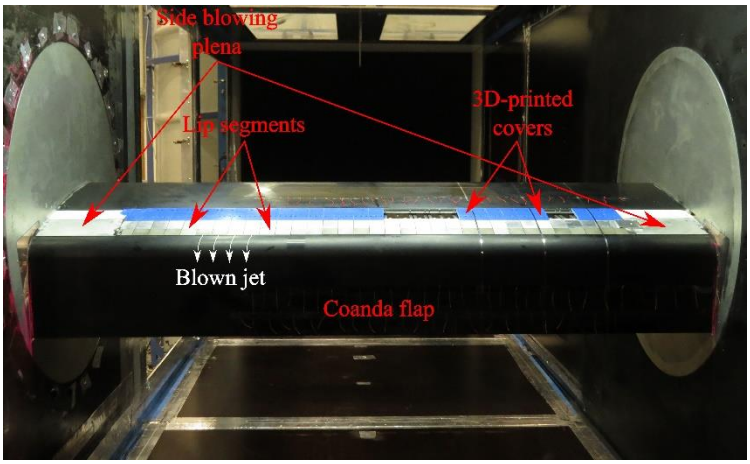

Fig. 1. The experimental model installed in the wind tunnel test section.

The experimental 2D model is a modified DLR-F15 airfoil (Fig. 1) with a chord length of $c = 600\,mm$, and a $1.3\,m$ span. It features a highly deflected Coanda flap and a drooped leading edge. The Coanda flap has a length of $c_{fl} = 0.25c$ (i.e. $c_{fl} = 150mm$) and is deflected by 65° for a landing configuration. The Coanda jet is blown over the flap shoulder through a $0.00067\,c$ gap. The jet is supplied through a plenum inside the model, which is connected on both sides of the model to a PoleStar PST120 refrigeration air dryer installed outside the tunnel and the building compressor, that delivers flow rates up to $1000\,l/s$ at $3\,bar$ pressure. To minimize side wall effects, the flow is kept attached near the tunnel walls using two separate Coanda actuation from a separate pneumatic feed.

The droop nose shape was reached through a parametric study that maximized the lift [34]. The geometry is morphed from the clean nose by deflecting the leading edge down by 90° over a length of $0.2c$, and increasing the leading edge thickness by 60%. The reference coordinate system, shown in figure 1, is that of the clean airfoil, where the leading edge coincides with the origin. Henceforth, all subsequent dimensions are with respect to this reference coordinate system.

B. Experimental Facilities

The experiment is carried out in the "Modell-Unterschallkanal Braunschweig" (MUB) at the Institute of Fluid Mechanics of the Braunschweig University of Technology. The wind tunnel is a low speed, closed circuit with interchangeable test sections. The test section used in this study has a cross section of $1.3 \times 1.3 \times 5$ meters, which allowed for a maximum flow velocity of $60\ m/s$ when empty. The current experiment is conducted at a reduced velocity of $\sim 50 m/s$ corresponding to a chord Reynolds number of 1.75 million. The wind tunnel is driven by a $300\ kW$ variable speed DC motor. The tunnel temperature is kept constant by a water-cooled heat exchanger in the settling chamber.

C. Design, Manufacturing and Testing of the Adaptive Lip Segments

An essential part of the active Coanda high lift system are the adaptive lip segments. The main requirements for the lip segments are an operating frequency of up to $300\ Hz$, an active displacement of $0.4\ mm$ at the tip and a high stiffness against $1\ bar$ plenum pressure. Besides the operation requirements, there are practical requirements dictated by the very limited design space of the wind tunnel model and the necessity for a light weight design to keep the resonance frequency of the system above $300\ Hz$. To accomplish the spanwise variation, the actuator lip is subdivided into 33 individually controllable segments each with a $29\ mm$ width. This segmentation is a compromise between aerodynamic resolution and mechanical system complexity.

Fig. 2. Final design of an actuated lip segment.

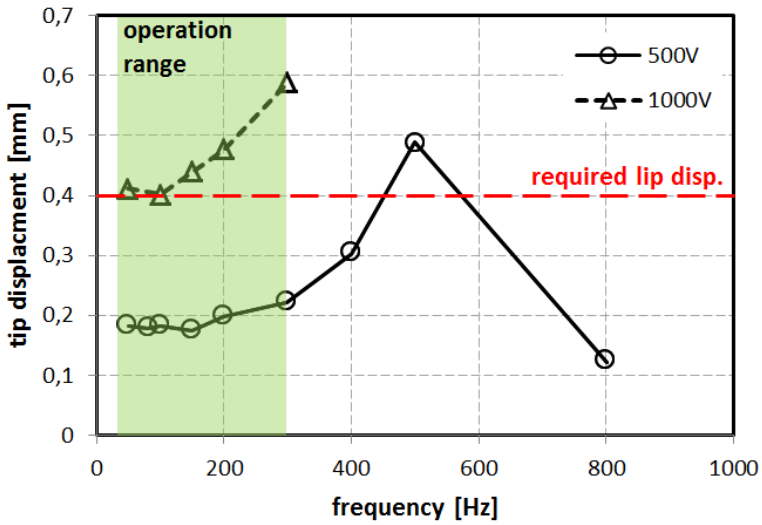

Fig. 3. Lip displacement at different frequencies and actuation voltages at a plenum pressure of 1 bar.

A systematic design study was carried out to identify the most suitable actuation concept. This included electromagnetic, pneumatic and piezoelectric actuation principles. The combination of a piezoelectric stack actuator with a compliant leverage was identified as the best design option for the given problem. Using an analytical model,

the principle lever ratios and dimensions were defined. The detailed design of the actuated lip was developed in an iterative process. Finite element models were used for stress analysis and to determine the deformation behavior of the lip under aerodynamic loads. During this phase several prototypes were built and tested with the help of 3D printing technologies to allow an evaluation of the concept at an early stage.

Fig. 2 shows the winning lip segment design. The lip segment is equipped with a high voltage piezoelectric stack actuator (type P-010.40 PI Ceramic) with a 56 mm length and a 10 mm diameter. This actuator generates a free displacement of 60 µm and has a blocking force of 2.2 kN. The lever mechanism translates this stroke into a 0.6 mm movement at the tip in the unloaded case and 0.4 mm in the loaded case (1 bar plenum pressure). The flexure hinge is composed of a carbon fiber laminate with a thickness of 0.5 mm. To reduce the weight of the lip, the main body is made of aluminum whereas the lip tip is made of hardened steel to provide sufficient stiffness against the aerodynamic loads.

To test the lip under aerodynamic loads a test rig with a pressurized plenum was build. The test rig allows the installation of three lip segments side by side. In Fig. 4 the measured frequency-dependent displacement of the actuated lip is presented for a range of actuation voltages. Over the relevant frequency range (marked in green) the required displacement of 0.4 mm at the lip tip can be achieved with a nominal actuation voltage of 1000 V. To determine the resonance frequency, the actuation voltage was reduced to avoid high resonant displacements. The diagram shows clearly that the resonance frequency is well above 300 Hz. The test rig was also used to determine the long time behavior of the lip segments. After 5×108 load cycles at full voltage and with a frequency of 300 Hz no reduction of the active performance was observed.

The tips of the lip segments are equipped with small neodymium magnets. In combination with integrated hall sensors below the skin of the Coanda flap a direct measurement of the lip deflection during the wind tunnel test is possible. Fig. 5 depicts the complete lip with all segments mounted onto a rail to facilitate the assembly and the later integration into the wind tunnel model. Manufacturing tolerances of the lip segments and of the attaching rail yielded slightly different performance amongst the different lip segments. This variation was addressed by calibrating each actuator against a laser scanner.

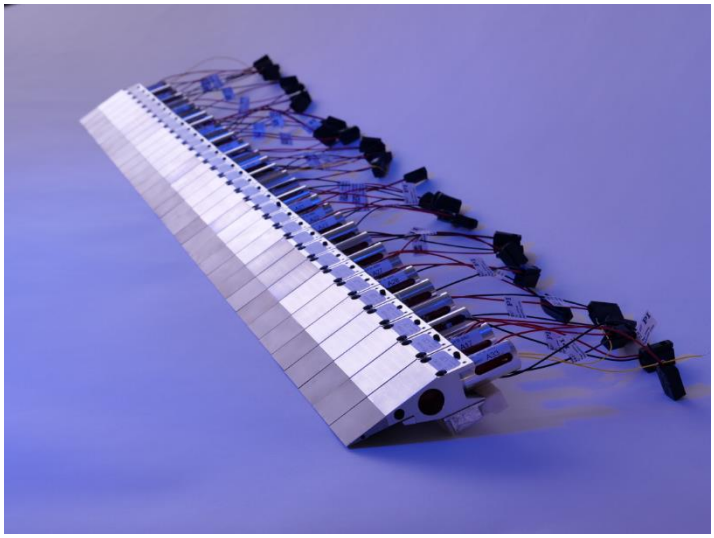

Fig. 4. 33 lip segments mounted onto an assembly rail before integration into the wind tunnel model.

D. Instrumentation

The lift coefficient is computed from the measured pressure distribution over the model surface. The pressure signals are collected from 196 surface pressure taps drilled across the model surface. Beside computing the lift coefficient, the pressure measurements are used to monitor the spanwise pressure distribution and hence to guarantee a two-dimensional flow along the span. The pressure measurements are acquired using a temperature compensated DTC Initium pressure measurement system with an ESP-64HD pressure scanner. The scanner has a 7 kPa pressure range and a full-scale accuracy of 0.03 %. For each measurement 400 samples are acquired at a sampling frequency of 100 Hz.

The wake dynamics are captured by eight time-resolved XCQ-093 Kulite pressure sensors distributed around the flap mid-span. The Kulites have a pressure range of 3.5×10^4 Pa and an accuracy of 0.1% of the full scale. For each

measurement 4000 samples are acquired at a sampling frequency of 1 kHz. The Kulite signals are also used as input for the machine-learning control.

In order to analyze the separation rate over the airfoil flap, yarn tufts are also used. A tape strip holding the tufts is attached at 80% flap chord length. The photos taken of the tufts illuminated with a black light provide visualization of the flow state over the flap under different actuation conditions.

III. Methodology

A. Lip Segments Motion and Test Cases

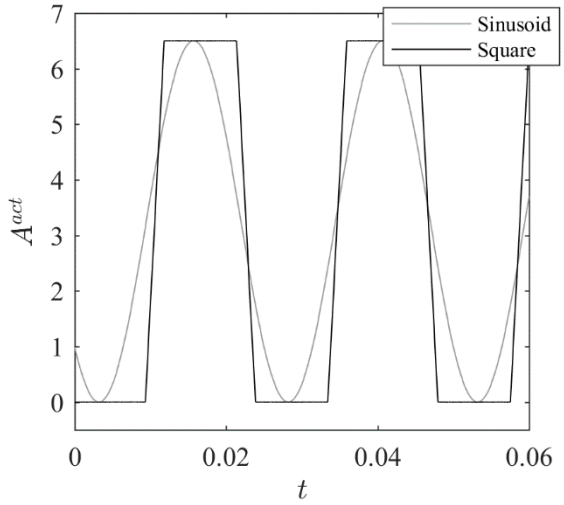

Fig. 5. A typical sinusoidal and square wave output signal.

Only one type of spanwise-varied actuation is investigated in the current work, which is the traveling wave. Other type of spanwise-varied actuation, such as the standing wave, will be investigated during a subsequent measurement campaign. The traveling wave motion is prescribed by the individual lip segments movement (b_i) as

$$\mathrm{b_i(t)} = \frac{\mathrm{A}}{2}(1 + \cos(\omega \mathrm{t} - \mathrm{kz_i})$$

where z_i denotes the ith lip along the spanwise direction, A is the normalized wave amplitude, ω is the angular frequency, $k = 2\pi/\lambda$ is the wavenumber, with λ the wavelength. The wave amplitude A is non-dimensionalized by the maximum possible amplitude, which is the amplitude that almost completely closes the jet slit. Hence, values close to one correspond to amplitude that are close to the maximum amplitude. To avoid damaging the actuators, the maximum allowed amplitude is limited to $A = 0.9$. It is worth to note that two-dimensional actuation, where all the lip segments are moving synchronously, is a special case of the traveling wave with $k = 0$. The phase velocity is defined as

$$\omega_b = \frac{\omega}{k}.$$

Let $W_{min} = 0.1U_\infty$ be the minimal considered phase velocity and $W_{max} = 2U_\infty$ be the maximum one. Let $\Lambda_{min} = (8/30)\mathrm{L}$ be the minimal considered wavelength and Λmax = 4L be the maximum one, where L is the model span length. The normalized wavelength range and the normalized phase velocity range can be expressed as

$$\lambda = \Lambda_{min} + (\Lambda_{max} - \Lambda_{min})\, p_\lambda$$
$$\omega_b = W_{min} + (W_{max} - W_{min})\, p_\omega.$$

Here,

$$p := (p_\lambda, p_\omega) \in [0,1] \times [0,1],$$

is the range of parameters sampled with the latin hypercube.

The actuation frequency is traditionally presented in its non-dimensional form F^+, defined as $F^+ = f \cdot c_f / U_\infty$, where $\omega = 2\pi f$. The actuation intensity is characterized by the momentum coefficient which is defined as

$$C_\mu = \frac{\dot{m}_{jet}(\mathrm{t}) \cdot v_{jet}(t)}{1/2 \cdot \rho_\infty \cdot U_\infty^2 \cdot S_{ref}}$$

where $v_{jet}(t)$ and $\dot{m}_{jet}(\mathrm{t})$ are the jet instantaneous velocity and instantaneous mass flow rate, ρ_∞ and U_∞ are the freestream density and velocity, and S_{ref} is the wing surface. The momentum coefficient is experimentally computed

using a Testo 6444 flowmeter and static pressure measurements in the plenum and at the jet exit [20]. To insure jet uniformity along the span, all thirty three lip segments are adjusted before the start of the measurement campaign. Due to the above-mentioned manufacturing tolerances of the lip segments and of the attaching rail, the jet momentum, measured by a pitot probe located ≈ 10 mm behind the blowing slot, could only be adjusted to within ±20%.

As the main objective of this study is to investigate possible lift gains, a moderate jet momentum coefficient, $C_\mu = 0.035$, is adopted for all measurements. This is motivated by the flow's partially separated state during steady blowing, which makes it more receptive to unsteady actuation [17, 18]. For the current preliminary results, only one angle of attack is comprehensively examined, 0◦, with three types of unsteady actuation: spanwise-synchronous with sinusoidal waves, spanwise-synchronous with square waves, and spanwise-varied with sinusoidal traveling waves. Typical sinusoidal and square wave output signals are presented in Fig. 5.

B. Machine Learning Control

Machine learning control is a model-free data-driven closed loop control methodology whose aim is to find the best control law $b = K(s)$ that minimizes a cost functional J, where s comprises the sensor signals [4, 5], b denotes the actuation signal whose dependence on s is expressed through the optimal control K. The optimization technique utilized is genetic programming which belongs to the larger group of evolutionary algorithms. These algorithms mimic natural evolution by repeatedly having a group of possible solutions (control laws) compete against each other. A group of possible solutions is usually referred to as one generation, while a single solution is called an individual. An algorithm implementing genetic programming starts with creating a random initial generation of a defined size. Each individual is assessed by testing its ability to control the system, which is quantified by $J(K)$. Once the performance of each control law is known, a second generation can be generated from the first through a set of genetic operations. These operations are replications, crossover and mutation. The chances of each of these operations being used is controlled by their respective probability P_r, P_c, and P_m. In addition, elitism preserves the best individuals in the next generation. The evolutionary process is repeated until a break criterion, such as a target fitness or a maximum number of generations, has been met. For more details, see [11].

The current work presents the initial results of machine learning control tests implemented on the wind tunnel experiment. To reduce complexity during these initial tests, only spanwise-uniform actuation is implemented. In other words, all lip segments are synchronized. For the current high-lift configuration, two simultaneous cost functionals to be minimized are considered: $J_1 = C_\mu$ and $J_2 = 1/C_l$. An additional objective is complexity, which encourages simplicity and robustness of the control laws. As the valves controlling the plenum pressure operate on a relatively long time-scale, the plenum pressure is kept constant and all variations in C_μ are obtained through mass flow rate fluctuations from the dynamic lip motion. The probability of genetic operations for the current campaign are $P_r = 0.3$, $P_c = 0.5$ and $P_m = 0.2$. The individuals are generated as expression trees made of user-defined nodes (sin, cos), basic operations (+, −, ×, /), constants and the sensor input $s(t)$. The input signal consists of the eight time-resolved pressure sensors (Kulite), which are enriched by their time delayed signal of about 4 ms, by their own time windowed variances and their respective differences. Such enrichment has been demonstrated to yield faster convergence and more physically-interpretable control laws [6]. To weed out bad individuals before evaluation and shorten the experimental evaluation time, all control laws are synthetically pretested by random signals in the expected range of their dependent sensors. Anything that produces an output that exceeded the range limit (7 V) more than 95% of the time is rejected and given a bad fitness value.

The entire process is executed with the National Instrument Compact Rio 9035 controller, through which the pressure input signals are read and the actuation commands are outputted. The genetic programming code is the Python-based Glyph software [35].

IV. Initial Results

A. Steady Blowing

For circulation control wings, increasing steady blowing has been repeatedly shown to increase the lift coefficient [17, 18]. This can be explained from the mechanisms behind the Coanda flap. The plane wall jet that emerges from a slit follows the surface and, depending on its momentum, increasingly attaches the flow over the flap. Steady mean equations of motion that take curvature into account prove that equilibrium is maintained by the centrifugal force being balanced by the pressure gradient that is normal to the mean streamlines. The mechanism causing separation is the entrainment of ambient fluid that is slowing the jet down, subject to the adverse pressure gradient from the flap knuckle shape at the hinge line toward the trailing edge [14]. Hence, increasing the actuation intensity causes the separation to gradually recede over the flap up to $C_\mu = 0.065$ where the flow becomes fully attached. At low blowing

intensities ($C_\mu = 0.015$) the flow is only partially attached over the flap. For high blowing intensities ($C_\mu = 0.065$) the flow is attached over the entire flap length. This gradual mitigation of separation and the added circulation result in steady lift gains, as shown in Fig. 7 for three mean steady blowing intensities: $C_\mu = 0$, 0.035, and 0.055. The lower stall angles with higher C_μ can be also observed.

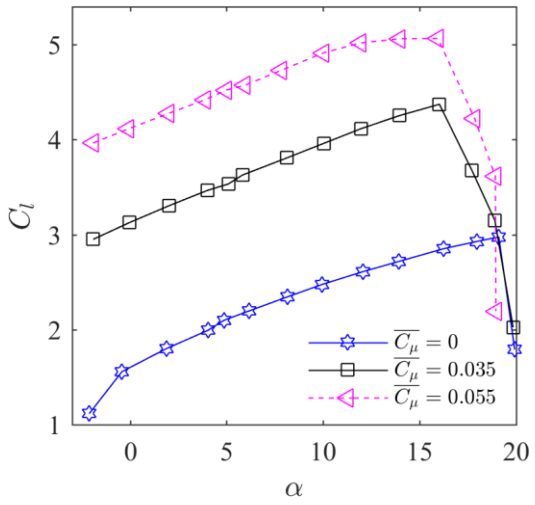

Fig. 6 Pressure coefficient distribution with increasing momentum coefficients at α = 0° and (a) Re= 1.0 × $10^6$and (b) Re= 1.5 × 10^6, respectively.

B. Two-Dimensional Spanwise-Synchronous Actuation

The effect of two-dimensional spanwise-synchronous actuation with mean blowing intensity $C_\mu = 0.035$ at $Re = 1.75 \times 10^6$ is presented in Fig. 7 for (a) sinusoidal and (b) square wave motion. The mean blowing intensity $C_\mu = 0.035$ is selected for its aerodynamic characteristics, where the flow is partially separated during steady actuation ($F^+ = 0$), and is thus more receptive to superimposed unsteady actuation. As the figure shows, the superposition of a periodic component has a clear impact on the aerodynamic performance. Depending on the actuation amplitude and actuation frequency, the lift coefficient can either increase or decrease. For the sinusoidal wave motion (Fig. 7 (a)), the highest lift gains with respect to steady blowing $\Delta C_l = C_l - C_{l,steady}$, are concentrated around the region of $F^+ \approx 0.125$ and $A \approx 0.86$ and reach $\Delta C_l \approx 0.19$. This lift gain region is relatively narrow, and is flanked by high lift losses at lower actuation frequencies. On the other hand, the lift gains for the square wave motion (Fig. 7 (b)) are more robust and are spread around a broader frequency range. The highest gains are similar to the sinusoidal wave results ($\Delta C_l \approx 0.20$), and are achieved similarly at around $F^+ \approx 0.125$ but at a smaller actuation amplitude of $A \approx 0.70$. Hence, for the square wave motion, the highest lift gains are achieved at amplitudes well below those required to completely open/close the slit. The optimal actuation frequency of $F^+ \approx 0.125$ for both wave motions is a sub-harmonic of the shedding frequency [19]. Interestingly, there is no observable lift sensitivity at the shedding frequency $St = 0.25$. It is not entirely clear why the shedding frequency and its sub-harmonic exhibit such distinct actuation sensitivity. Field wake measurements and spectral analysis should pinpoint the responsible physical mechanisms behind these observations. Time-resolved PIV measurements will be conducted in the near-future to investigate this phenomenon.

Unlike previous experimental investigations in the water tunnel [17], the current measurements exhibit different lift gain sensitivities to actuation for varying angle of attack range. Fig. 8 presents the lift coefficient over a range of angles of attack for a non-dynamically actuated and three dynamically-actuated cases at their respective optimal settings at $\alpha = 0°$ for $C_\mu = 0.035$. At first, the lift gains remain relatively constant with larger angles until $\alpha \approx 8°$. Thereafter, the lift gains for all dynamically-actuated cases gradually shrink until they become losses at the maximum angle of attack $\alpha_{max} \approx 16°$. Additional measurements in both the wind and water tunnel are required to shed light on this discrepancy.

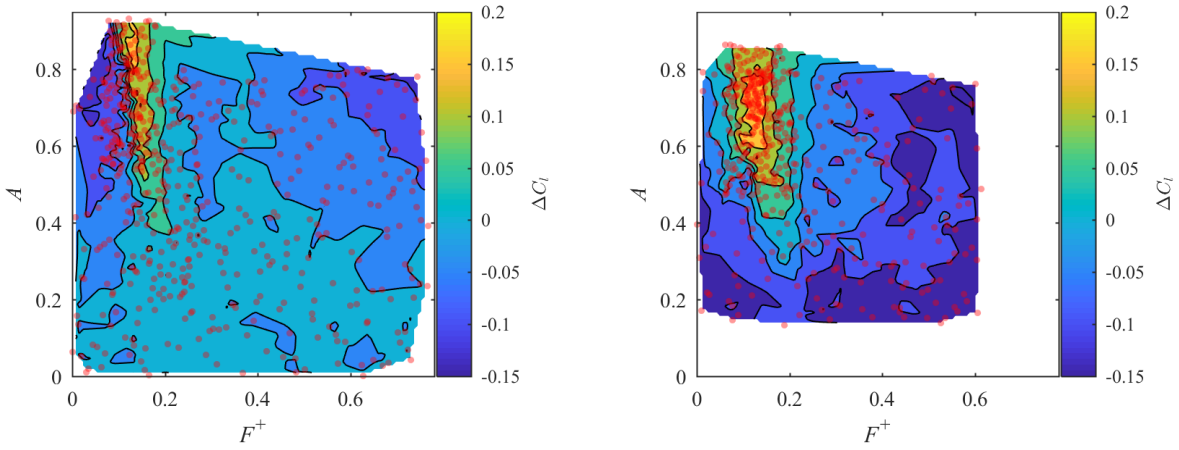

Fig. 7. Lift gain distributions with respect to steady blowing at $C_\mu = 0.035$ for a range of actuation frequencies and amplitudes for (a) sinusoidal and (b) square wave motion. The red dots denote the measured values.

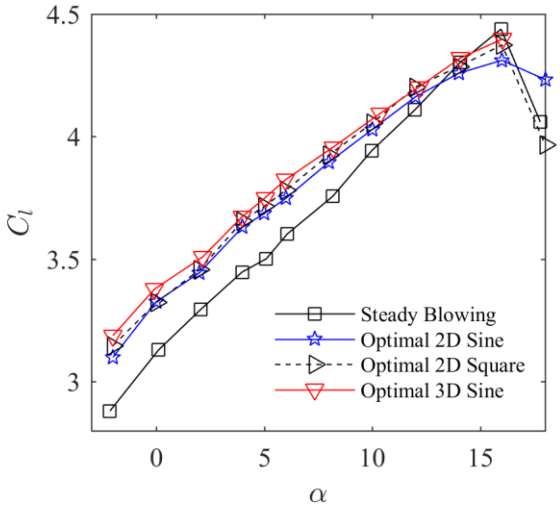

Fig. 8. C_l vs. α for a non-dynamically actuated and three dynamically-actuated cases at their respective optimal settings at $\alpha = 0°$ for $C_\mu = 0.035$ and Re= 1.75×10^6.

C. Three-Dimensional Traveling Wave Actuation

The effect of three-dimensional spanwise-varied actuation with sinusoidal motion and a mean blowing intensity $C_\mu = 0.035$ at $Re = 1.75 \times 10^6$ is presented in Fig. 9 for the traveling wave at $\alpha = 0°$. Also shown are two slices at (b) a constant frequency $F^+ = 0.018$, and at (c) a constant wavelength $k = 1.67$, which coincide with the optimum setting. The mean blowing intensity is the same as for the two-dimensional actuation analysis in section IV B.

Similar to two-dimensional sinusoidal actuation, the highest lift gains are observed at relatively high amplitude (A) and low actuation frequency (F^+). The maximum lift gain reaches $\Delta C_l \approx 0.25$, which is slightly better than the best two-dimensional actuation. The highest gains are achieved at a similar amplitude $A \approx 0.87$, but at a lower actuation frequency $F^+ \approx 0.018$ than the spanwise-synchronous actuation. The optimum wavelength is $k \approx 1.67$. These values correspond to a slow traveling wave with a wavelength of $\lambda \approx 2.89\,L$. It is not entirely clear at this point what the significance of this optimal wave is. At this point, we can only attribute the lift gains to favorable interactions between spanwise and longitudinal vortices. It is worth to note the sporadic coverage of the measured actuation parameter space, as seen in Figs. 9 (b) and (c). This originates from the traveling wave definition (§III A), which does not linearly map from the sampled space $p := (p_\lambda, p_\omega) \in [0,1] \times [0,1]$ to the physical space k, F^+.

Assessing the lift gains between the two-dimensional and the three-dimensional actuation, it is evident that three-dimensional actuation has a clear benefit over the two-dimensional one. In other words, the superposition of phase-shifted longitudinal vortices yield an additional lift increase of $\Delta C_l \approx 0.05$ over the spanwise periodic vortex. With the implementation of individual lip segment control and traveling wave with square motion, further lift gains in both spanwise-synchronous and spanwise-varied actuation can be expected.

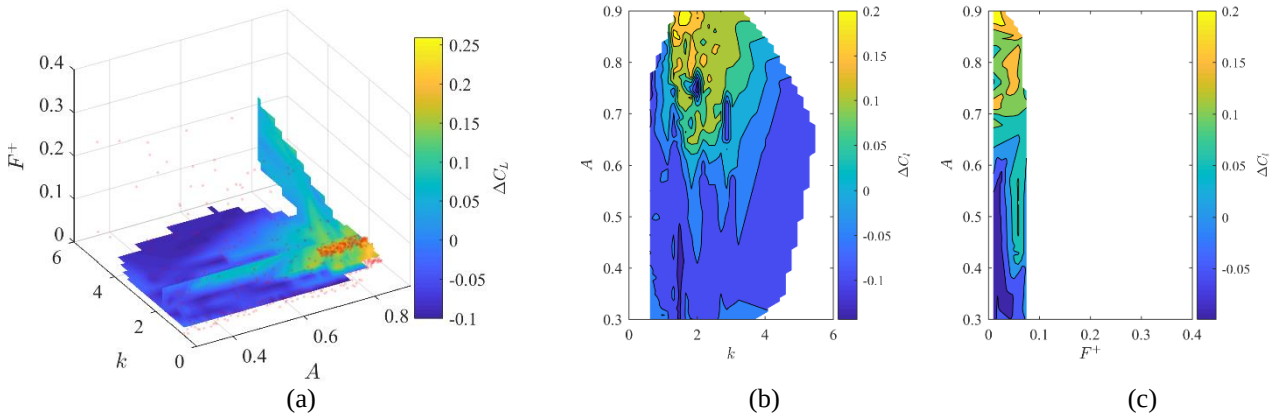

Fig. 9. (a) Lift gain distributions with respect to steady blowing at $C_\mu = 0.035$ for a range of actuation parameters for a traveling wave. The red dots denote the measured values. Also shown are two slices at (b) a constant frequency $F^+ = 0.018$, and at (c) a constant wavelength $k = 1.67$.

D. Machine Learning Control

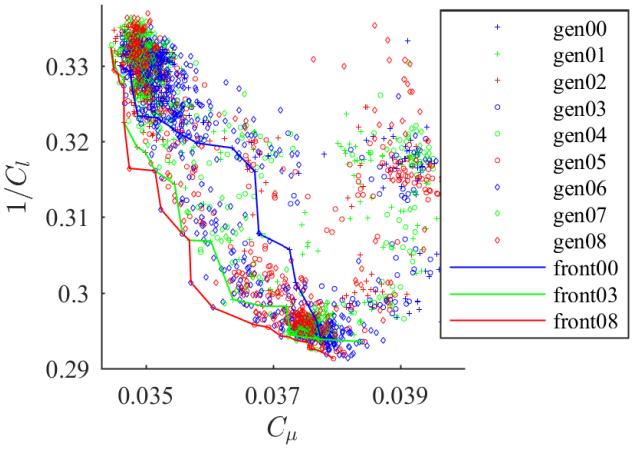

Fig. 10. The effect of the steady momentum coefficient on the lift coefficient over a range of angles of attack at Re= 1.75 × 10^6.

The evolution of the two cost functions with increasing number of individuals is shown as a Pareto plot in Fig. 10 for eight generations. All random control laws of the first generation are seen to be ineffective, i.e. produce only cost functions which are worse than the steady blowing case. Considering the large search space created by the many ways one can arrange the node functions, sensor and constants, it is not surprising that a Monte-Carlo process with 150 individuals is ineffective. With higher generations the Pareto front shifts to the lower left corner, thus minimizing both cost functionals. Convergence is reached after the 8th generation, after which the Pareto front exhibited no substantial enhancement in four generations from the eighth to 11th generation. Compared to the best two-dimensional spanwise synchronous open control at $C_\mu = 0.035$, machine learning control did not achieve any additional lift gains. It is suspected that some variation (decrease) in the actuator stiffness and its fastening to the model towards the end of the measurement campaign may have introduced actuation errors that reduced the effectiveness of the genetic

programming. With the planned hardware improvements, further aerodynamic gains in open and closed-loop control are expected.

V. Work to be completed

The results shown here are preliminary and mostly restricted to two blowing intensity, at one angle of attack. In the completed paper, more blowing intensities as well as more angles of attack will be examined. Improvements to the jet uniformity has been completed and is expected to improve the open- and closed-loop control performance. A more detailed analyses of the mechanisms behind the lift gains shall also be presented.

Acknowledgments

We acknowledge the funding and excellent working conditions of the Collaborative Research Centre (CRC 880) 'Fundamentals of High Lift of Future Civil Aircraft' supported by the Deutsche Forschungsgemeinschaft (DFG) and hosted at the Technical University of Braunschweig.

References

[1] Greenblatt D., Wygnanski I., "The control of flow separation by periodic excitation," Progress in Aerospace Sciences, Vol. 36, No. 7, 2000, pp. 487-545. doi: 10.1016/S0376-0421(00)00008-7

[2] Barros, D., Borée, J., Noack, B. R., Spohn, A., and Ruiz, T., "Bluff body drag manipulation using pulsed jets and Coanda effect," Journal of Fluid Mechanics, Vol. 805, 2016, pp. 422-459. doi: 10.1017/jfm.2016.508

[3] Chabert, T., Dandois, J., and Garnier, A. , "Experimental closed-loop control of separated-flow over a plain flap using extremum seeking," Experiments in Fluid, Vol. 57 , No. 37, 2016. doi: 10.1007/s00348-016-2123-y

[4] Brunton, S. L. and Noack, B. R., "Closed-loop turbulence control: Progress and challenges", Appl. Mech. Rev., Vol. 67, No. 5, Article 050801, 2015, pp. 1–48

[5] Gautier, N., Aider, J. L., Duriez, T., Noack, B. R., Segond, M., and Abel, M.,"Closed-loop separation control using machine learning," Journal of Fluid Mechanics, Vol. 770, 2015, pp. 442-457.

[6] Duriez, T., Brunton, S. L., and Noack, B. R., "Machine Learning Control — Taming Nonlinear Dynamics and Turbulence," Springer, 2016.

[7] Höll, T., Günther, B., and Thiele, F. , "Numerical Investigation of Segmented Actuation Slits for Active Separation Control of a High-Lift Configuration," AIAA 2009-887, 2009.

[8] Höll, T., Wassen, E., and Thiele, F., "Active Separation Control on a High-Lift Configuration Using Segmented Actuation Slits," AIAA 2010-4249, 2010.

[9] Höll. T., Job, A. K. V., Giacopinelli, P., and Thiele F., "Numerical Study of Active Flow Control on a High-Lift Configuration," Journal of Aircraft, Vol. 49 , No. 5,pp. 1406-1422 , 2012.

[10] Davidson, I. M., "Aerofoil boundary layer control system," British Patent, 913, 754, 1960.

[11] Koza, J. R., "Genetic Programming: On the Programming of Computers by Means of Natural Selection," Cambridge, MA: MIT Press ,1992.

[12] Lachmann, G. V., "Boundary layer and flow control: its principles and application," New York: Pergamon Press ,1961.

[13] Wood, N. J. and Nielson, J. N., "Circulation control airfoils - Past, present and future," AIAA Paper-85-0204, 1985.

[14] Neuendorf, R. and Wygnanski, I., " On a turbulent wall jet flowing over a circular cylinder," Vol. 381, pp. 1–25, 1999.

[15] Nielson, J. N. and Biggers, J., " Recent progress in circulation control aerodynamics," AIAA Paper-87-0001, 1987.

[16] Englar, R., "Circulation control pneumatic aerodynamics: blown force and moment augmentation and modifications; past, present, and future," AIAA Paper-2000-2541, 2000.

[17] Semaan R., El Sayed M. Y., and Radespiel R., "Sparse Model of the Lift Gains of a Circulation Control Wing With Unsteady Coanda Blowing," Accepted for publications in: Active Flow and Combustion Control 2014, Springer, 2018.

[18] El Sayed M. Y., and Semaan R. and Radespiel R., "Open Loop Control on a Coanda Flap Water Tunnel Model," AIAA 2017-3247, 2017. 12

[19] El Sayed M. Y., Sattler S., Radespiel R., Semaan R., "Wake Characterization behind a Circulation Control Wing," Experiments in Fluids 58:144, 2017.

[20] El Sayed M. Y., Beck N., Kumar P., Semaan R., Radespiel R., "Challenges in the Experimental Quantification of the Momentum Coefficient of Circulation Controlled Wings,' In: Dillmann A. et al. (eds) New Results in Numerical and Experimental Fluid Mechanics XI. Notes on Numerical Fluid Mechanics and Multidisciplinary Design, vol 136. Springer, 533–543, 2018.

[21] Sexstone, M. G., Huebner, L. D., Lamar, J. E., McKinley, R. E., Torres, A. O., Burley, C. L., Scott, R. C. and Small, W. J., "Synergistic airframe-propulsion interactions and integrations," Tech. Rep. NASA/TM-1998-207644. NASA Langley Research Center; Hampton, VA United States, 1998.

[22] Smith, A. M. O., "High-lift aerodynamics," Journal of Aircraft, Vol. 12, No. 6, pp. 501-530, 1975.

[23] Jensch, C., Pfingsten, K. C., Radespiel, R., Schuermann, M., Haupt, M. and Bauss, S., "Design aspects of a gapless high-lift system with active blowing," In 58. Deutscher Luft- und Raumfahrtkongress , Aachen, Germany , 2009.

[24] Radespiel, R., Pfingsten, K.-C. and Jensch, C., “Flow analysis of augmented high-lift systems,” In Hermann Schlichting-100 Years (ed. R. Radespiel, C. C. Rossow and B. W. Brinkmann), pp. 168-189, 2009.
[25] Oyler, T. E. and Palmer, W. E., “Exploratory investigation of pulse blowing for boundary layer control,” North American Rockwell: Columbus division, Tech. Rep. No.: NR72H-12, 1972.
[26] Walters, R. E., Myer, D. P., and Holt, D. J., “Circulation control by steady and pulsed blowing for a cambered elliptical airfoil,” West Virginia University, Aerospace Engineering, Tech. Rep. No.: TR-32, 1972.
[27] Jones, G. S., Viken, S. A., Washburn, A. E., Jenkins, L. N. and Cagle, C. M., “An active flow circulation controlled flap concept for general aviation aircraft applications",” AIAA paper-2002-3157, 2002.
[28] Woszidlo R, Wygnanski IJ , “Parameters governing separation control with sweeping jet actuator,” . In: AIAA-2011-3172, 2011.
[29] Seifert, A., Greenblatt, D. and Wygnanski, I. J., “Active separation control: an overview of Reynolds and Mach number effects",” Aerospace Science and Technology, Vol. 8, No. 7, pp. 569-582, 2004.
[30] Mahmood, S. and Radespiel, R., “Zonal Improved Delayed Detached-Eddy Simulationof Vortex Generator Jets at High Reynolds Numbers for Aeronautical Flows,” CEAS Aeronautical Journal, ISSN 1869-5582, Vol. 4, No. 2 ,pp. 203-222, 2013.
[31] Johnston J. P. and Nishi M., “Vortex generator gets-means for flow separation control,” AIAA Journal, Vol. 28, No. 6, pp. 989-994, 1990.
[32] Ortmanns J., Bitter M., and Kähler C. J., “Dynamic vortex structures for flow-control applications,” Experiments in Fluids, Vol. 44, No. 3, pp. 397- 408, 2008.
[33] Hsiao, F. B., Liang, P. F., and Huang, C. Y., “High-incidence airfoil aerodynamics improvement by leading-edge oscillating flap,” Journal of aircraft, Vol. 35, No. 3, pp. 508-510, 1998.
[34] Burnazzi, M. and Radespiel, R., “Design and Analysis of a Droop Nose for Coanda Flap Applications,” AIAA Journal of Aircraft, Vol. 51, No. 5, pp. 1567-1579 , 2014. doi: 10.2514/1.C032434
[35] Quade, M., Gout, J. and Abel, M., “Glyph - Symbolic Regression Tools”, arXiv:1803.06226 [cs.MS], 2017, doi: 10.5281/zenodo.1156654, url: https://github.com/Ambrosys/glyph